VIP Germanium Nanotubes

DOI: 10.1002/anie.201103062

Germanium Nanotubes Prepared by Using the Kirkendall Effect as Anodes for High-Rate Lithium Batteries**

*Mi-Hee Park, YongHyun Cho, Kitae Kim, Jeyoung Kim, Meilin Liu, and Jaephil Cho**

The specific energy and the charge/discharge rate (power) of the existing batteries severely limit their use in many applications, such as electric vehicles and smart grids where batteries are needed to store energy from renewable sources of intermittent nature (for example, solar and wind).[1,2] While replacing a graphitic carbon anode by metallic Si, Ge, or Sn[3–5] may increase the anode capacity about three times, the rapid capacity fading during cycling due to large volume change has severely hindered their applicability to practical lithium-ion cells with operating voltages of between 3 and 4.3 V.

Germanium has gained much attention as a promising anode material for lithium-ion batteries because of its excellent lithium-ion diffusivity (400 times faster than in Si), high electrical conductivity (10^4 times higher than Si),[6–11] and large theoretical specific capacity (ca. 1600 $mAhg^{-1}$, corresponding to $Li_{4.4}Ge$). However, mechanical stresses induced by the volume changes during cycling result in pulverization and exfoliation from current collector,[1–5] leading to capacity fading and poor cycling life. Among various approaches to minimize the mechanical stresses induced by volume change, the use of nanotubes (NTs) is proven to be most effective in accommodating the volume changes of electrode materials during cycling.[1] Accordingly, anodic aluminum oxide (AAO) templates have been commonly used to produce NTs of many different materials.[12–17] Unfortunately, this approach results in very low yields, produces NTs with non-uniform wall thicknesses, and is vulnerable to contamination by impurities involved in the reaction process.

[*] M.-H. Park, Y. Cho, Prof. J. Cho
Interdisciplinary School of Green Energy
Ulsan National Institute of Science and Technology (UNIST)
Ulsan, 689-798 (Korea)
E-mail: jpcho@unist.ac.kr
Homepage: http://jpcho.com
Dr. K. Kim, Dr. J. Kim
Battery R&D Center, LG Chem., Ltd.
104-1, Moonji-dong, Yuseong-gu, Daejeon, 305-380 (Korea)
Prof. M. Liu
School of Materials Science and Engineering
Georgia Institute of Technology
771 Ferst Drive, N.W. Atlanta, GA 30332-0245 (USA)

[**] This work was supported by the Converging Research Center Program (2010K000984). This research was also supported by the MKE (The Ministry of Knowledge Economy), Korea, under the ITRC (Information Technology Research Center) support program supervised by the NIPA (National IT Industry Promotion Agency) (NIPA-2011-C1090-1100-0002). M.-H.P. acknowledges the TJ Park Doctoral Fellowship (POSCO TJ Park Foundation).

Supporting information for this article is available on the WWW under http://dx.doi.org/10.1002/anie.201103062.

In 2004, a unique process based on the Kirkendall effect[18] was successfully used to convert metal nanoparticles into hollow metal oxide and sulfide. Kirkendall voids form as a consequence of the difference in diffusion fluxes of atoms across an interface in a diffusion couple at elevated temperatures.[19–23] When outward diffusion of one atom is much faster than the inward diffusion of another, vacancies are created on the side with higher diffusivity. These vacancies can coalesce into voids under proper conditions. To date, however, similar structures of semiconductors (e.g., Ge and Si) are yet to be produced.

Herein we present a high-yielding synthetic method for fabrication of ultralong Ge NTs from core–shell Ge–Sb nanowires (NWs) by utilizing the Kirkendall effect at 700 °C. The Ge NTs displayed exceptionally high rate capability of up to 40 C (40 Ag^{-1}) while maintaining a reversible capacity of >1000 $mAhg^{-1}$ over 400 cycles with minimal capacity fading when paired with a $LiCoO_2$ cathode in a lithium-ion cell.

TEM images showing the evolution of a Ge NW (**1a**) to a Ge NT (**1e**) by the Kirkendall effect are given in Figure 1 a–e. First, a mixture of antimony acetate and polyvinyl pyrrolidone (PVP) was coated on the Ge NW (**1b**). The amount of antimony acetate and PVP were varied to adjust the coating concentration of antimony to about 2 wt % of the Ge NWs used. Upon annealing at 700 °C, voids start to form inside the core–shell interface (**1c**) and continue to grow until the conversion is completed (**1d**). Finally, nanotubular morphology is formed after annealing for 5 h (**1e**), resulting in Ge NTs with diameters varying from 200 to 250 nm (see the Supporting Information, Figure S1–S4 for more detailed morphology evolution from NW to NT). More importantly, the wall thickness of the Ge NTs after annealing for 5 h is relatively uniform (ca. 40 nm; Supporting Information, Figure S5 c). The selected area diffraction pattern indicates that the NTs are amorphous (Supporting Information, Figure S5 c inset). Furthermore, to enhance the long-term stability, the Ge NTs were exposed to C_2H_2 gas for the last 20 min of the 5 h annealing to introduce a thin-film carbon coating on the surface of the Ge NTs (Supporting Information, Figure S5).

These results show that Ge NTs are formed by a multiple-step process (see Figure 1 f with 2D cross-sectional views of the NW/NT at each step of the conversion): a) coating Ge NWs with an antimony precursor; b) Ge atoms diffuse outward, leaving voids inside the NWs (note that germanium can react with a variety of metals, such as Au, Ag, Bi, and Sb, with lower atomic diffusivity,[24] thereby creating a void between the inner wire and the outer tube); c) the outer germanium layer continues to diffuse and completely separates from antimony and a portion of Ge NW; d) the inner

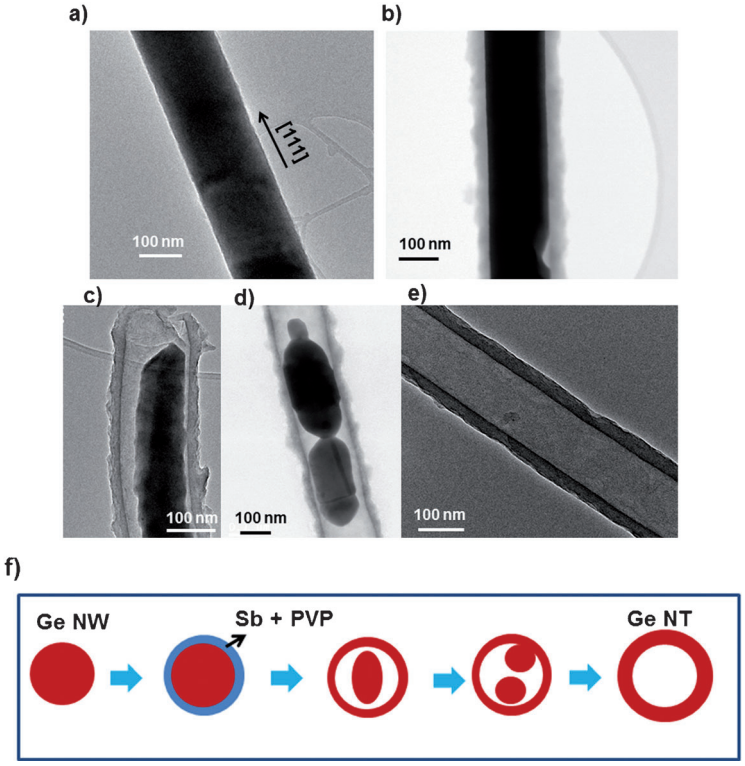

Figure 1. a,b) TEM images of a Ge NW and a Ge NW coated with antimony acetate and PVP, respectively; c,d) TEM image of the coated Ge NW in (b) after annealing for 2 and 3 h at 700 °C, respectively, and e) TEM image of the coated Ge NW after annealing for 5 h at 700 °C. f) The evolution of Ge NWs to Ge NTs by utilizing the Kirkendall effect. 2D cross-sectional views are given for the NW/NT at each step of the conversion captured by the TEM images shown in (a) to (e).

Ge NW transforms into antimony nanoparticles in a process that is very similar to the formation of fragmentized nanoparticles in the voids of Ag_2Se NTs converted from Ag NWs coated with CSe_2.[25] Voids began to develop and merge at the boundary because the high concentration of defect and surface energy associated with the boundary favor the formation of the voids there.[25] Unlike the isotropic growth of voids in the spherical nanoparticles, however, the voids in our case grow along the longitudinal direction. We believe such behavior is due to the high concentration of antimony atoms adhered to the [111] direction of Ge NW promotes the diffusion of germanium atoms along the longitudinal axis, leading to an anisotropic growth along [111] direction; e) germanium nanoparticles disappear completely upon long-term annealing at 700 °C to finally form Ge NTs.

Figure 2a shows the voltage profiles of the Ge NTs versus lithium at a cycling rate of 0.2 C (200 mAg^{-1}) between 0 and 1.5 V. The discharge and charge capacity of the first cycle were 1341 $mAhg^{-1}$ and 1022 $mAhg^{-1}$, respectively, corresponding to a coulombic efficiency of 76 %. This is lower than that for Ge NWs (ca. 88 %),[26] which is most likely due to enhanced formation of solid electrolyte interface (SEI) layer on the NTs during the first cycle since the EDXS of the NTs annealed for 5 h showed negligible amount of oxygen contamination (< 3 wt %; Supporting Information, Figure S6). However, compared to a previous report on Ge NWs prepared by a direct VLS growth using GeH_4 that showed a coulombic efficiency of about 33 %,[27] our Ge NTs demonstrates noticeably improved efficiency, which may be attributed to the carbon coating that minimized surface oxidation of germanium. It has been reported that the irreversible capacity loss of the lithium reactive alloys is closely related to some side reactions between the active material and the electrolyte (especially $LiPF_6$).[28] We believe that the contribution of antimony to capacity was negligible owing to its low content.

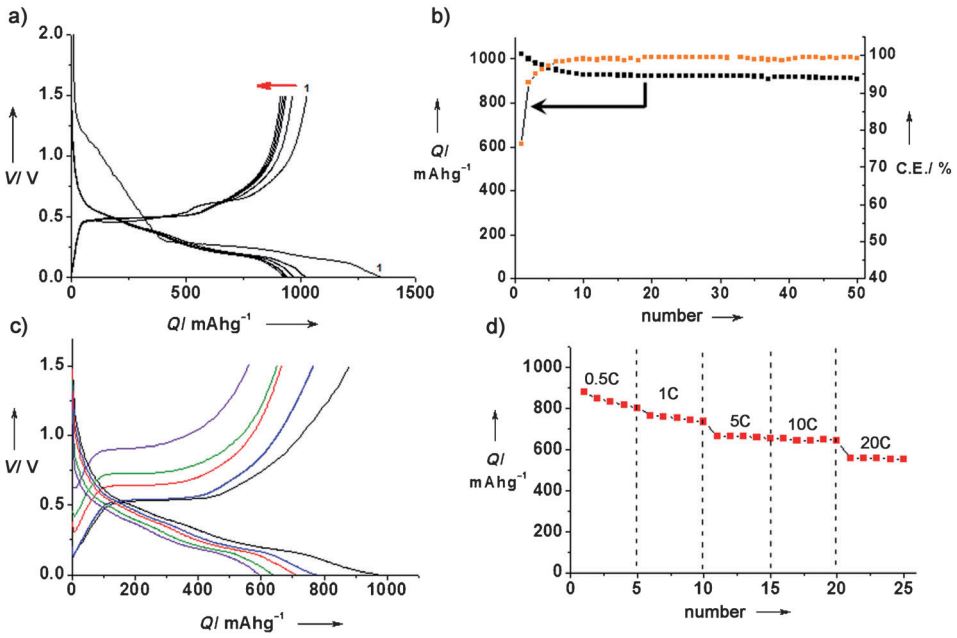

Figure 2. a) Voltage profiles of Ge NTs in coin-type lithium cells after 1, 5, 20, 30, 40, and 50 cycles (cycle 1 marked; progression shown by red arrow) between 0 and 1.5 V at a charge/discharge rate of 0.2 C. b) Plot of charge capacity (lithium de-alloy) and coulombic efficiency (C.E.) of (a) as a function of cycle number. c) Voltage profiles of Ge NTs in the coin-type lithium cells at different C rates (0.5C black, 1C blue, 5C red, 10C green, and 20C purple) between 0 and 1.5 V. Charge and discharge rates were the same. d) Plot of charge capacity versus cycle number at different C rates. All cells were cycled at 21 °C.

As seen in Figure 2b, the capacity retention of the Ge NTs was about 8 % after 50 cycles at a cycling rate of 0.2 C, showing a reversible capacity of 1002 $mAhg^{-1}$ with coulombic efficiency of > 99 %. The enhanced coulombic efficiency (> 99 %) after the first

cycle is attributed to the thin carbon layer, which minimizes the direct contact between germanium and the electrolyte, facilitating the formation of a stable SEI layer on both the inner and the outer surface of the Ge NTs. It has been reported that bare silicon or germanium nanoparticles undergoing lithium alloying and dealloying reactions are continually exposed to the electrolyte owing to the recurrent generation of new active surfaces that were previously passivated by stable surface films, resulting in capacity fading during cycling.[29] Compared with Ge NWs,[26] the capacity retention of Ge NTs was improved by more than 20%, which is most likely due to the absence of inhomogeneous volume expansion in the coexistence regions of phases within different lithium concentrations, which occurs in crystalline phase. Accordingly, amorphous Ge NTs enable homogenous volume expansion and contraction, whereas the hollow space inside the Ge NTs acts as a buffer for volume expansion.

Figure 2c shows voltage profiles of the Ge NTs in the rage of 0 V and 1.5 V vs. Li/Li^+ at different cycling rates (with the same rates for both charge and discharge). The obtainable charge capacities (after lithium was removed) were 965, 765, 702, 629, and 580 $mAhg^{-1}$ at a rate of 0.5, 1, 5, 10, and 20C (20 Ag^{-1}), respectively. The capacity retention at 20C rate is 60%, which is exceptionally high among all metallic anodes ever reported.[1–11,26] For instance, the obtainable capacity for Ge NWs became very small above 6C rate for either charge or discharge.[26] Moreover, the obtainable capacity at each cycling rate remained relatively constant (Figure 2d), suggesting excellent cycling stability. These performance characteristics are far superior to those previously reported for germanium-based systems.[6–11] Furthermore, it should be noted that the electrode density (which was often ignored in previous studies) of the Ge NTs is relatively high. Although Ge NTs has a porous morphology, the density of an electrode consisting of Ge NTs, carbon black, and binder (with a weight ratio of 80:10:10) is about 1.2 gcc^{-1}. Hence, its volumetric capacity is estimated to be about 1226 $mAhcc^{-1}$, based upon its initial charge capacity.

As the cell resistance of the lithium half-cell (>1 KΩ) was typically much higher than that of the full cells (<50 mΩ), a rate capability test at higher rates showed higher polarization and subsequent rapid capacity decrease in the half cell than in a full cell. Accordingly, meaningful rate capability (up to 40C or 40 Ag^{-1} rate) should be obtained from balanced full cells. In this study, the rate capability and cycling life of the Ge NT-based anodes were demonstrated in pouch-type lithium-ion cells using $LiCoO_2$ as the cathode. To date, while many high capacity anode nanomaterials have been reported (for example, silicon- and tin-based nanomaterials), only a few were tested in lithium-ion cells.[17,30] The best rate capability demonstrated by Si NT-based anodes in lithium-ion cells was about 5C (or 15 Ag^{-1}) with capacity retention of about 92%.[17] In contrast, the Ge NTs-based anodes in lithium-ion cells (with a $LiCoO_2$ cathode) demonstrated a rate capability of about 40C (or 40 Ag^{-1}) for both charge and discharge between 3 and 4.3 V (Figure 3a), with obtainable capacity of 716 $mAhg^{-1}$ (corresponding to about 70% capacity retention). The exceptionally high rate capability of the Ge NTs is attributed to their unique morphology (ca. 40 nm thick wall and about 170 nm pore diameter) for rapid mass and charge transport, together with high lithium-ion diffusivity (400 times faster than in silicon) and excellent electrical conductivity (10^4 times higher than silicon).[6] More surprisingly, capacity retention was about 98% after more than 400 cycles (Figure 3b,c); the first and the 400th charge capacities were 1020 and 1002 $mAhg^{-1}$, respectively, which was based on three different cells tested. This result represents a significant enhancement in performance over the latest Si-NT/$LiCoO_2$ cell (ca. 92% capacity retention after 200 cycles[17]).

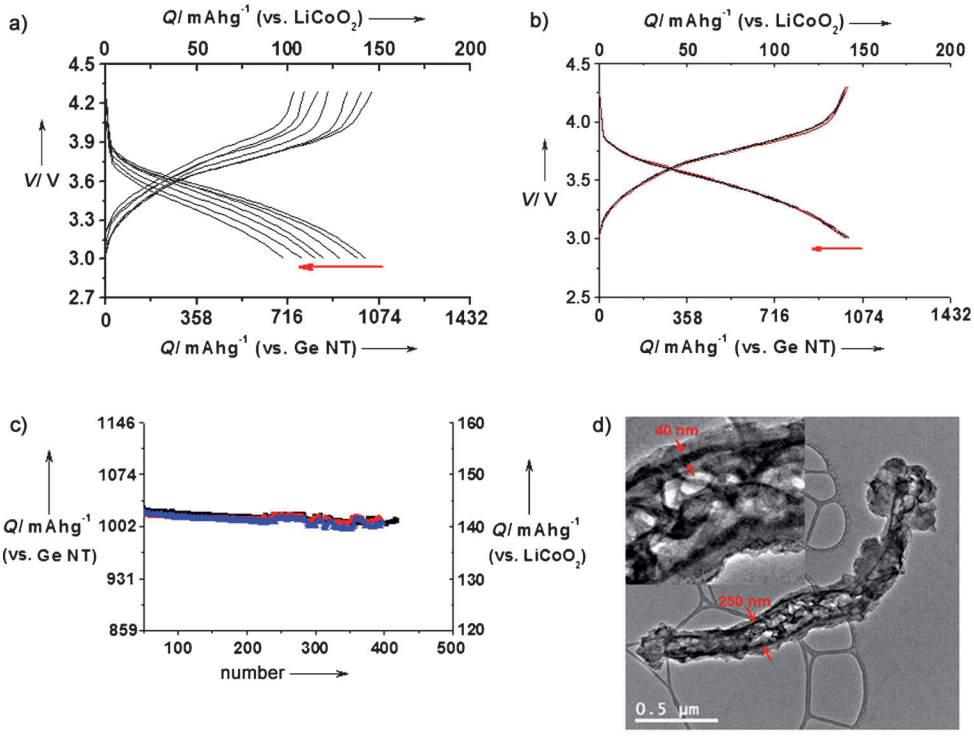

Figure 3. a,b) Voltage profiles of pouch-type lithium-ion cells: a) cycled between 3 and 4.3 V at different C rates: 1C, 5C, 7C, and, 20C, 30C, and 40C (charge rate = discharge rate), b) after 1, 150, 300, and 400 cycles between 3 and 4.3 V (charge rate 0.5C, discharge rates 1C). c) Plot of capacity versus cycle number in three different lithium-ion cells. d) TEM image of a Ge NT after 400 cycles; inset: expanded view. As the NT was extracted from the composite electrode, its surface was covered by binder and carbon black.

We believe that the superior performance of the Ge NTs is attributed to the unique synthetic method utilizing the Kirkendall effect, which produces tubular morphology with uniform wall thickness. In contrast, the Si NTs derived from AAO template had much less uniform wall thickness, resulting in capacity fading owing to inhomogeneous volume expansion and contraction. In fact, cycled Si NTs exhibited partial distortion of tubular morphology.[17] TEM examination of the Ge NTs, however, revealed no observable distortion after battery testing (Figure 3d). On the other hand, composite silicon-in-carbon tubes exhibited stable and reversible capacity of 800 $mAhg^{-1}$ up to 250 cycles in lithium half cells at a current rate of 1700 mAg^{-1}.[31]

In conclusion, Ge NTs have been synthesized using a high-yield method. The Ge NTs demonstrated exceptionally high rate capability with excellent capacity retention and stability over 400 cycles, suggesting that Ge NTs are ideally suited as anodes for a new generation of high-power lithium-ion batteries for a wide range of applications.

Experimental Section

Ge nanowires were synthesized under Ar in a three-neck flask on a Schlenk line as described elsewhere.[26] To coat Sb on the Ge NWs, polyvinyl pyrrolidone (PVP; MW = 55000, Aldrich) were added to ethanol and Ge NWs were subsequently added. The mixture was thoroughly mixed before addition of antimony acetate (Aldrich, 99.6%), followed by drying at 80°C and then annealing at 700°C for 1–8 h under mixture gas flow ($Ar/H_2 = 90:10$ vol%). The amount of Sb acetate and PVP were varied to adjust coating concentration of Sb to about 2 wt% of the Ge NWs used (a typical batch size was about 20 g). To deposit an amorphous carbon coating on the surface of annealed Ge NTs, C_2H_2 gas was introduced at the last 30 min of the annealing process at 700°C.

Fabrication of lithium half cells and lithium-ion cells: The anodes for the test cells were made of Ge NTs, Super P carbon black, and polyvinylidone fluoride (PVDF) binder (Solef) in a weight ratio of 80:10:10. The slurry was prepared as described elsewhere[28] by thoroughly mixing an *N*-methyl-2-pyrrolidone solution (NMP; Aldrich, 99.9%) of PVDF, carbon black, and the active anode material. The coin-type half cells (2016R size), prepared in a helium-filled glove box, contained Ge NTs, Li metal, a microporous polyethylene separator, and an electrolyte solution of 1.1M $LiPF_6$ in ethylene carbonate/ethyl methyl carbonate/dimethyl carbonate (EC/EMC/DMC; 3:3:4 vol.%; LG Chem., Korea) without using any additives. The capacity was estimated based only on the active material used (that is, carbon-coated Ge NTs including Sb).

Pouch type lithium-ion batteries with $LiCoO_2$ cathodes[32] were prepared with a nominal capacity of about 300 mAh. The Ge NT anodes were assembled using automatic cell assemblage lines in a dry room with a H_2O level of < 100 ppm. The test cathode consisted of 92 wt% cathode material, 3 wt% polyvinylidene fluoride (PVDF), and 5 wt% carbon black. The test anode consisted of 80 wt% Ge NTs, 10 wt% PVDF, and 10 wt% natural graphite. As the N/P ratio (negative/positive dimensional ratio) was fixed at 1.01, the area-normalized capacities of both cathode and anode were set at 15 and 15.15 $mAh\,cm^{-2}$, respectively. Loading levels for the cathode and anode were fixed at 3.4 gcc^{-1} and 1.2 gcc^{-1}, respectively. Each cell was aged for 24 h at room temperature before commencing the electrochemical tests, and the internal resistance of as-prepared lithium ion cells was (45 ± 5) mΩ. The cycling tests of the cells were performed with three different cells between 4.3 and 3 V at various charge and discharge rates of constant current. Sample characterization methods using XRD, TEM, Raman, and CHNS elemental analyses are provided in the Supporting Information.

Received: May 4, 2011
Revised: June 10, 2011
Published online: August 31, 2011

Keywords: anodes · germanium · Kirkendall effect · lithium battery · nanotubes

[1] K. T. Lee, J. Cho, *Nano Today* **2011**, *6*, 28.
[2] G.-A. Nazari, G. Pistoia, *Lithium Batteries: Science and Technology*, Kluwer/Plenum, Boston, **2004**.
[3] a) K. Evanoff, A. Magasinski, J. Yang, G. Yushin, *Adv. Energy Mater.* **2011**, *1*, 495; b) A. Magasinski, P. Dixon, B. Hertzberg, A. Kvit, J. Ayala, G. Yushin, *Nat. Mater.* **2010**, *9*, 353.
[4] C. K. Chan, Y. Cui, *Nat. Nanotechnol.* **2008**, *3*, 31.
[5] G. Cui, L. Gu, L. N. Kaskhedikar, P. A. van Aken, P. A. J. Maier, *Electrochim. Acta* **2010**, *55*, 985.
[6] J. Graetz, C. C. Ahn, R. Yazami, B. Fultz, *Electrochem. Solid-State Lett.* **2003**, *6*, A194.
[7] M. G. Kim, J. Cho, *J. Electrochem. Soc.* **2009**, *156*, A277.
[8] G. Cui, L. Gu, L. Zhi, N. Kaskhedikar, P. A. van Aken, K. Mullen, J. Maier, *J. Adv. Mater.* **2008**, *20*, 3079.
[9] H. Lee, H. Kim, S. Doo, J. Cho, *J. Electrochem. Soc.* **2007**, *154*, A343.
[10] H. Lee, C. Choi, Y. K. Sun, J. Cho, *J. Phys. Chem. B* **2005**, *109*, 20719.
[11] M. H. Park, K. Kim, J. Kim, J. Cho, *Adv. Mater.* **2010**, *22*, 415.
[12] R. Tenne, C. N. R. Rao, *Philos. Trans. R. Soc. London Ser. A* **2004**, *362*, 2099.
[13] M. Niederberger, H.-J. Muhr, F. Krumeich, F. Bieri, D. Günther, R. Nesper, *Chem. Mater.* **2000**, *12*, 1995.
[14] W. Stober, A. Fink, E. Bohn, *J. Colloid Interface Sci.* **1968**, *26*, 62.
[15] Y. Ono, K. Nakashima, M. Sano, Y. Kanekiyo, K. Inoue, S. Shinkai, M. Sano, J. Hojo, *Chem. Commun.* **1998**, 1477.
[16] W. J. Lee, M. H. Park, Y. Wang, J. Y. Lee, J. Cho, *Chem. Commun.* **2010**, *46*, 622.
[17] M.-H. Park, M. G. Kim, J. Joo, K. Kim, J. Kim, S. Ahn, Y. Cui, J. Cho, *Nano Lett.* **2009**, *9*, 3844.
[18] Y. Yin, R. M. Rioux, C. K. Erdonmez, S. Hughes, G. A. Somorjal, A. P. Alivisatos, *Science* **2004**, *304*, 711.
[19] X. Liang, X. Wang, Y. Zhuang, B. Xu, S. Kuang, Y. Li, *J. Am. Chem. Soc.* **2008**, *130*, 2736.
[20] H. J. Fan, M. Knez, R. Scholz, D. Hesse, K. Nielsch, M. Zacharias, U. Gosele, *Nano Lett.* **2007**, *7*, 993.
[21] Q. G. Li, R. M. Penner, *Nano Lett.* **2005**, *5*, 1720.
[22] H. Peng, C. Xie, D. T. Schoen, K. McIlwrath, X. F. Zhang, Y. Cui, *Nano Lett.* **2007**, *7*, 3734.
[23] H. J. Fan, M. Knez, R. Scholz, K. Nielsch, E. Pippel, D. Hesse, M. Zacharias, U. Gosele, *Nat. Mater.* **2006**, *5*, 627.
[24] a) P. Leveque, J. S. Christensen, A. Kuznetsov, B. G. Svensson, A. N. Larsen, *J. Appl. Phys.* **2002**, *91*, 4073; b) M. Werner, H. Mehrer, H. D. Hochheimer, *Phys. Rev. B* **1985**, *32*, 3930.
[25] C. H. B. Ng, H. Tan, W. Y. Fan, *Langmuir* **2006**, *22*, 9712.
[26] M.-H. Seo, M.-H. Park, K. T. Lee, K. Kim, J. Kim, J. Cho, *Energy Environ. Sci.* **2011**, *4*, 425.
[27] C. K. Chan, X. F. Zhang, Y. Cui, *Nano Lett.* **2008**, *8*, 307.
[28] H. Uono, B.-C. Kim, T. Fuse, M. Ue, J.-I. Yamaki, *J. Electrochem. Soc.* **2006**, *153*, A1708.
[29] a) N.-S. Choi, Y. Yao, Y. Cui, J. Cho, *J. Mater. Chem.* **2011**, *21*, 9825; b) J. Cho, *J. Mater. Chem.* **2010**, *20*, 4009.
[30] M. G. Kim, S. Sim, J. Cho, *Adv. Mater.* **2010**, *22*, 5154.
[31] B. Hertzberg, A. Alexeev, G. Yushin, *J. Am. Chem. Soc.* **2010**, *132*, 8548.
[32] M. Jo, S. Jeong, J. Cho, *Electrochem. Commun.* **2010**, *12*, 992.

